Chinese Physics B

Proximity-induced Negative Magnetoresistance and Anomalous Hall Effect in Monolayer Graphene/CrSBr Heterojunctions

To cite this article before publication: Bin Dai *et al* 2026 *Chinese Phys. B* in press https://doi.org/10.1088/1674-1056/ae64d4

Proximity-induced Negative Magnetoresistance and Anomalous Hall Effect in Monolayer Graphene/CrSBr Heterojunctions

Bin Dai(戴彬)[1,2,#], *Ke Zhu*(祝轲)[2,#], *Chenyu Bai*(白晨宇)[2,3,#], *Yechao Han*(韩烨超)[3], *Guojing Hu*(胡国静)[3], *Ruwen Wang*(王汝文)[2,3], *Senhao Lv*(吕森浩)[2], *Haisen Liu*(刘海森)[1,2], *Zhen Zhao*(赵振)[2], *Jianchen Lu*(卢建臣)[1,*], *Hui Guo*(郭辉)[2,3,*], *Haitao Yang*(杨海涛)[2,3], *Hong-Jun Gao*(高鸿钧)[2,3]

[1]*Faculty of Materials Science and Engineering, Kunming University of Science and Technology, Kunming 650093, China*

[2]*Beijing National Center for Condensed Matter Physics and Institute of Physics, Chinese Academy of Sciences, Beijing 100190, China*

[3]*School of Physical Sciences, University of Chinese Academy of Sciences, Beijing 100049, China*

[#] These authors contributed equally to this work

[*] Corresponding author. E-mail: guohui@iphy.ac.cn;

[*] Corresponding author. E-mail: jclu@kust.edu.cn

Abstract

The integration of graphene with magnetic insulators to invoke the magnetic proximity effect provides a powerful route toward spintronic devices that preserve graphene's exceptional transport characteristics. A persistent challenge, however, is the identification of magnetic substrates that are both air-stable and capable of forming high-quality van-der-Waals interfaces. Here, we present the magnetotransport investigation of monolayer graphene coupled to a layered A-type antiferromagnetic semiconductor CrSBr nanoflake, which is notable for its high Néel temperature (~132 K) and outstanding environmental stability. High-quality heterojunctions are obtained via a dry-transfer technique to ensure atomically clean interface. Pronounced negative magnetoresistance and anomalous Hall effect in graphene are observed, arising from the suppression of spin-disorder scattering induced by the proximity exchange field from the CrSBr layer. Moreover, the heterojunction exhibits clear two-frequency Shubnikov-de Haas oscillations, evidencing the emergence of Fermi surface reconstruction of the monolayer graphene. Our results demonstrate that antiferromagnetic CrSBr can impose a robust magnetic proximity effect that manipulates the spin degrees of freedom in graphene, opening new opportunities for spintronic functionalities in two-dimensional materials.

Keywords: magnetic proximity effect, negative magnetoresistance, anomalous hall, Shubnikov de Haas oscillation

PACS: 72.80.Vp, 73.43.Qt, 85.75.-d

Introduction

Two-dimensional (2D) materials continue to reshape the landscape of spin-based electronics. Graphene, with its exceptionally high carrier mobility (>10^5 cm^2 V^{-1} s^{-1}) and long spin diffusion length(~30 μm) that persist up to room temperature, provides an ideal platform for low-dissipation spin transport.[1,2] However, the absence of intrinsic magnetic order in pristine graphene limits its direct applications in spintronics devices. A widely adopted strategy to overcome this limitation is the magnetic proximity effect (MPE), whereby an exchange field is induced in graphene through intimate contact with a magnetic insulator.[3–9] The resulting exchange splitting can break time-reversal symmetry and generate spin-polarized carriers in the graphene.[10]

Compared to ferromagnetic materials, antiferromagnetic materials possess a net zero magnetic moment, thereby avoiding stray fields that could degrade device performance while offering strong stability against external magnetic perturbations.[11–16] Theoretical models predict that exchange interactions at the graphene/antiferromagnet interface can break time-reversal symmetry and induce an effective exchange field, leading to spin band splitting in graphene.[17] Among the van-der-Waals (vdW) magnets, the layered A-type antiferromagnet CrSBr stands out because of its relatively high Néel temperature (T_N~132 K) and robust environmental stability, whereas other 2D magnets such as CrI_3 are known to be unstable under ambient conditions.[18–21] Recent studies have demonstrated that monolayer CrSBr can impose a sizable exchange field on an adjacent graphene layer, manifested as a gate-tunable spin polarization and a measurable exchange shift of 27–32 meV in the

graphene band structure.[22] However, comprehensive transport signatures, particularly quantum effects under high magnetic fields, that directly link the proximity-induced exchange to modifications of the Fermi surface remain scarce.

In this work, we report the magnetotransport properties of a high-quality monolayer graphene/CrSBr heterojunction. Our measurements reveal a clear MPE in monolayer graphene induced by CrSBr nanoflake, giving rise to a pronounced negative magnetoresistance (NMR) of up to -23%. Furthermore, the presence of exchange field modifies the well-established Dirac spectrum of graphene, resulting in an unusual electronic transport behavior in the quantum oscillation regime. The two-frequency Shubnikov-de Haas (SdH) oscillations are observed in the heterojunction at low temperatures. In addition, the transverse Hall resistance exhibits a pronounced deviation from the linear dependence expected for a single-carrier Dirac system, evidencing the existence of anomalous Hall effect (AHE). Our results confirm the capability of antiferromagnetic CrSBr to engineer spin-selective electronic structures in graphene, paving the way for developing high-performance, multifunctional spintronic architectures.

Experiment details

The high-quality CrSBr single crystals were synthesized through a chemical vapor transport (CVT) method.[23,24] High-purity Cr powder (99.95%), $CrBr_3$ powder (99%) and S powder (99.9995%) were thoroughly mixed and sealed in a quartz ampoule under high-vacuum conditions. The ampoule was placed in a two-zone horizontal furnace,

with the hot zone and the cold zone maintained at 950℃ and 850℃, respectively, for 72 hours. Finally, the CrSBr single crystals were obtained after the furnace was cooled naturally to room temperature.

Large-area monolayer graphene and CrSBr nanoflakes were exfoliated onto the SiO_2/Si substrate that was pretreated with oxygen plasma. Subsequently, a polymer stack was employed to selectively transfer the exfoliated flakes. The monolayer graphene was picked up by using a *h*-BN nanoflake and then precisely released onto the pre-exfoliated CrSBr nanoflake.[25] The polymer residue was removed by immersing the stacked heterojunction in acetone.

The Hall bar devices of the heterojunction were fabricated using standard e-beam lithography (Raith 150), followed by deposition of Cr/Au electrodes (5 nm/35 nm). Prior to metal deposition, the top *h*-BN layer was selectively removed by SF_6 reactive ion etching (RIE) to expose the graphene contact regions. The thicknesses of heterojunctions were determined using a commercial atomic force microscope (AFM, Oxford Instruments Cypher S). Raman spectra were acquired using a WITec ALPHA300R system. Electrical transport measurements were conducted using a standard four-terminal configuration within a Physical Property Measurement System (PPMS, Dyna-Cool, Quantum Design).

Results and discussion

Figure 1(a) illustrates crystal structures of monolayer graphene and a CrSBr nanoflake, where vdW interactions are formed between the two layers after the

heterostructure is assembled using a dry-transfer technique. The device configuration discussed in this work is shown in Fig. 1(b). Figure 1(c) presents the Raman spectra of the monolayer graphene, *h*-BN, CrSBr, and the heterojunction, all measured on a SiO_2 /Si substrate. The characteristic Raman peaks of both CrSBr and monolayer graphene are clearly preserved in the spectrum of the heterojunction, indicating the formation of high-quality vdW interface between two layers. Figure 1(d) shows the AFM image of the device and the corresponding height profile extracted along the white line, showing a thickness of ~3.2 nm for the CrSBr nanoflake.

The magnetic properties of the synthesized CrSBr bulk crystal were first characterized. Temperature-dependent magnetic susceptibility measurements under zero-field-cooling (ZFC) and field-cooling (FC) procedures reveal a sharp cusp at T_N = 132 K (Fig. 2(a)), consistent with previous reports and signaling the onset of antiferromagnetic order.[18] A weak ferromagnetic-like feature emerges below 27.5 K, which may arise from the existence of defects in crystals.[26,27] Figure 2(b) displays the field-dependent magnetization with the external field applied along the crystallographic *c* axis. Below T_N, the magnetic state of CrSBr undergoes a transition from canted antiferromagnetism to field-polarized ferromagnetism as the external field increases beyond the saturation field B_{sat}, which has been reported to be comparable in the bulk and few-layer CrSBr.[27,28]

Figure 2(c) presents the longitudinal magnetoresistance ratio (MRR = R(B)/R(0)) measured under the out-of-plane magnetic field. Across the entire temperature range, the heterojunction exhibits clear NMR. At 180 K, which is above T_N, the sample

exhibits a broad NMR response, whereas below T_N, the NMR shows a distinct two-regime behavior. Taking the curve measured at 2 K as an example, the MR drops steeply as the magnetic field increases up to about 2.1 T and then gradually saturates at higher fields. The characteristic transition field B_{trans} (~2.1 T) is marked by the dashed line in Fig. 2(c). Such two-regime behavior, an initial rapid drop followed by a plateau, suggests a strong coupling between the magnetic order of CrSBr and the charge carriers in the adjacent monolayer graphene.

Several well-known mechanisms can give rise to NMR in low-dimensional systems, such as Kondo effect, weak localization(WL), and magnetic scattering.[29–32] The NMR induced by the Kondo effect typically follows a quadratic field dependence $MR \propto B^2$, which is not observed in our device. Thus, the Kondo effect can be ruled out. In the case of the WL in 2D materials, the conductivity is expected to exhibit a logarithmic temperature dependence, $\sigma_{xx} \propto \ln T$, which is also absent in the present measurements.

To quantify the correlation between the magnetic ordering of CrSBr and the transport response of heterojunction, we extracted two characteristic fields, B_{sat} and B_{trans}, as a function of temperature (Fig. 2(d)). The two data sets nearly coincide at each temperature and exhibit essentially identical temperature dependence. This quantitative agreement indicates that the MR response of the heterojunction is governed by the magnetic ordering of the CrSBr nanoflake. Below T_N, CrSBr develops antiferromagnetic order that becomes stronger upon cooling. Through MPE, an exchange field is induced in the adjacent monolayer graphene, leading to the spin

polarization of its charge carriers. This spin polarization enhances the spin-dependent scattering. While the external magnetic field aligns the magnetic moments in CrSBr, spin-disorder scattering is progressively suppressed, resulting in the observed NMR. Once B exceeds B_{trans}, the CrSBr spins become nearly fully polarized, the exchange field in graphene reaches its maximum, and the spin-related scattering channel exhibits field-independent, giving rise to the plateau observed in the magnetoresistance.

Figure 2(e) displays the magnitude of the maximum NMR evaluated at B_{trans} as a function of temperature. The NMR magnitude does not follow a simple monotonic trend, instead, it displays a pronounced valley between 20 K and 40 K, where the curve evolves from a weak temperature dependence at higher temperatures to a steep increase upon further cooling. Similar low-temperature weak ferromagnetic signals have been reported in several independent investigations of CrSBr and have been attributed to magnetic defects (e.g., Cr vacancies, stacking faults, or canting of the antiferromagnetic sublattices) that generate uncompensated moments within an antiferromagnetic host.[28] The sudden increase of the NMR therefore likely reflects the combined effect of the enhanced magnetic order in the pristine lattice and the emergence of defect-related magnetic moments that further modulate the spin-dependent scattering in the monolayer graphene.

To further investigate the influence of the CrSBr layer on the charge transport in graphene, we examined the Hall response of the heterojunction below T_N. Figure 3(a) shows the Hall resistivity ρ_{xy} as a function of the out-of-plane magnetic field at various temperatures. For magnetic fields exceeding 2.1 T, ρ_{xy} exhibits a negative

linear dependence, as evidenced by the ordinary Hall effect (OHE) with electron-type charge carrier. From the linear high-field Hall response, we extracted the carrier density n_e and mobility μ using a single-band model. As shown in Fig. 3(b), the carrier density remains nearly constant with increasing temperature, while the mobility increases significantly.

In the low-field region (| B | < 2.1 T), a distinct deviation from linearity is observed. This nonlinearity cannot be explained by a two-band conduction model and is therefore attributed to the AHE in graphene induced via the magnetic proximity effect. After subtracting the linear OHE background, we extracted the anomalous Hall conductivity at each temperature. As shown in Fig. 3(c), the magnitude of anomalous Hall conductivity increases monotonically with temperature, suggesting a close connection between the AHE and carrier scattering processes. To elucidate the underlying mechanism, we plotted σ^A against σ_{xx} on a double-logarithmic scale (Fig. 3(d)). The data follows a clear power-law scaling, with a linear fit yielding a slope of 2.1, i.e. $\sigma^A \propto \sigma_{xx}^{2.1}$. This quadratic scaling, combined with the moderate σ_{xx} values (10^3~10^4 Ω^{-1}cm^{-1}) firmly places the system in the side-jump regime, particularly in the presence of the magnetic disorder or strong spin-orbit coupling. Therefore, we attribute the observed AHE primarily to a side-jump scattering mechanism associated with the magnetic proximity effect induced by CrSBr.

The SdH effects are observed in the graphene/CrSBr heterojunction when the magnetic field exceeds 5 T. Figure 4(a) displays the temperature dependence of the magnetoresistance ratio under magnetic field ranging from 0 to 9 T. Pure oscillatory

component ΔR_{xx} is extracted by subtracting a polynomial background (Fig. 4(b)). As shown in Fig. 4(c), the fast Fourier transform (FFT) spectra reveal two frequencies at $F_\alpha = 90$ T, $F_\beta = 171$ T. According to the Onsager relation $F = (\hbar/2\pi e)A_F$, these frequencies correspond to the extremal cross-sectional area (A_F) of the Fermi pockets perpendicular to the magnetic field. The corresponding areas are determined to be 0.00857 and 0.0163 Å^{-2} for F_α and F_β, respectively.

The effective mass can be extracted by fitting the temperature dependence of the oscillation amplitude using the thermal damping term R_T in the Lifshitz-Kosevich (LK) formula, $\Delta R_{xx} \propto \frac{5}{2}\sqrt{\frac{B}{2F}} R_T R_D R_S cos[2\pi(F/B + \gamma - \delta)]$, where $R_T = (\lambda m^* T/B) / \sinh(\lambda m^* T/B)$, $R_D = \exp(-\lambda m^* T_D/\mu_0 H)$, $R_S = cos(\pi m^* g^*)$.[33,34] Here, $m^*$is cyclotron mass, T_D is Dingle temperatures, g^* is the effective g-factor, and the constant $\lambda = 2\pi^2 k_B m_e / e\hbar \approx 14.69\ T/K$. The extracted effective masses corresponding to the two frequencies are shown in Fig. 4(d). Both values are remarkably small, consistent with characteristic of Dirac fermions in graphene. The extracted parameters for the two Fermi pockets are summarized in table 1.

We observed that the quantum mobility extracted from SdH oscillations is significantly larger than the Hall mobility in the present system. This substantial discrepancy can be understood by considering the multiband nature of charge transport. The Hall mobility derived from a single-band model reflects a weighted average of the densities and mobilities of all carriers. In our case, the two small Fermi pockets resolved by SdH oscillations exhibit higher quantum mobility. However, due to their low carrier

density, their contribution to the overall conductivity is negligible. Meanwhile, a high-density, low-mobility carrier likely exists that dominates the Hall response but remains undetected in the SdH oscillations.

Consequently, the Hall mobility is suppressed by these low-mobility carriers, while the SdH oscillations selectively probe the clean, high-mobility pockets, yielding a larger quantum mobility. Such a scenario is well-documented in other multiband systems, confirming that the observed discrepancy is physically consistent.[35,36]

The phase factor $\gamma - \delta$ from the LK formula is directly related to the Berry phase, where δ equals to 0 for the 2D system and ± 1/8 for the 3D system.[37,38] Determining the Berry phase therefore provides insights into the topology of the electronic bands. Accordingly, we plotted the Landau fan diagram, as shown in Fig. 4(e). The two oscillations corresponding to different frequencies can be separated by applying a band-pass filter. The Landau indices (n) are assigned to the maxima of R_{xx} because the oscillations remain in the low field limit.[39] According to the Lifshitz-Onsager relationship $n = \frac{F}{B} + \gamma - \delta$, the slope of the linear fit between n and $1/B$ yields the oscillatory frequency, while the intercept offers the information about the Berry phase. As shown in Fig. 4(e), the intercepts for F_α and F_β are determined to be 0.479 and 0.327, respectively, indicating a 2D Fermi surface for the α pocket and a 3D Fermi surface for the β pocket. The two intercepts correspond to Berry phases of approximately -0.04 π and -0.1 π, both close to 0, indicating a trivial band topology. Figure 4(f) shows a two-frequency LK fit for the SdH signals, where the excellent

agreement with the experimental data confirms the reliability of the extracted parameters.

The observation of two distinct SdH frequencies provides direct evidence for the Fermi surface reconstruction in monolayer graphene induced by the adjacent CrSBr layer. These phenomena result from the collective contribution of the MPE and charge transfer at the interface. Through MPE, the exchange from CrSBr splits the Dirac cone of graphene into two spin-polarized sub-bands, breaking time-reversal symmetry and lifting the spin degeneracy. Simultaneously, charge transfer from the CrSBr layer leads to n-type doping in the monolayer graphene, shifting the Fermi level above the Dirac point. The combined effects of exchange splitting and charge transfer results in multiple Fermi pockets, giving rise to the two observed SdH oscillations. Recent first-principles calculations have confirmed this band structure reconstruction at the monolayer graphene/CrSBr interface, revealing both the exchange-induced spin splitting and charge transfer effects.[38,39] This rigid band shift caused by charge transfer is also consistent with the nearly temperature-independent n-type carrier density derived from the single-band Hall analysis. The agreement between Hall transport and quantum oscillation results thus provides strong evidence for proximity-induced spin polarization and Fermi surface reconstruction in the graphene/CrSBr heterojunction.

Conclusion

In conclusion, we report a magnetotransport study of high-quality graphene/CrSBr heterojunctions, demonstrating an efficient spin injection and band structure engineering in graphene via the magnetic proximity effect. The devices exhibit a

pronounced NMR reaching -23% and a clear AHE below the Néel temperature of CrSBr. Magnetotransport measurements further reveal SdH oscillations with two distinct frequencies, providing direct evidence for the Fermi surface reconstruction in graphene. Our results demonstrate that antiferromagnetic CrSBr can induce substantial exchange splitting and Fermi surface reconstruction in adjacent graphene, establishing graphene/CrSBr heterojunction as a promising platform for spintronics devices.

Acknowledgment

The work is supported by grants from the National Key Research and Development Projects of China (2022YFA1204100), the National Natural Science Foundation of China (62488201, 52572188), the Innovation Program of Quantum Science and Technology (2021ZD0302700) and the China Postdoctoral Science Foundation (E5BK081).

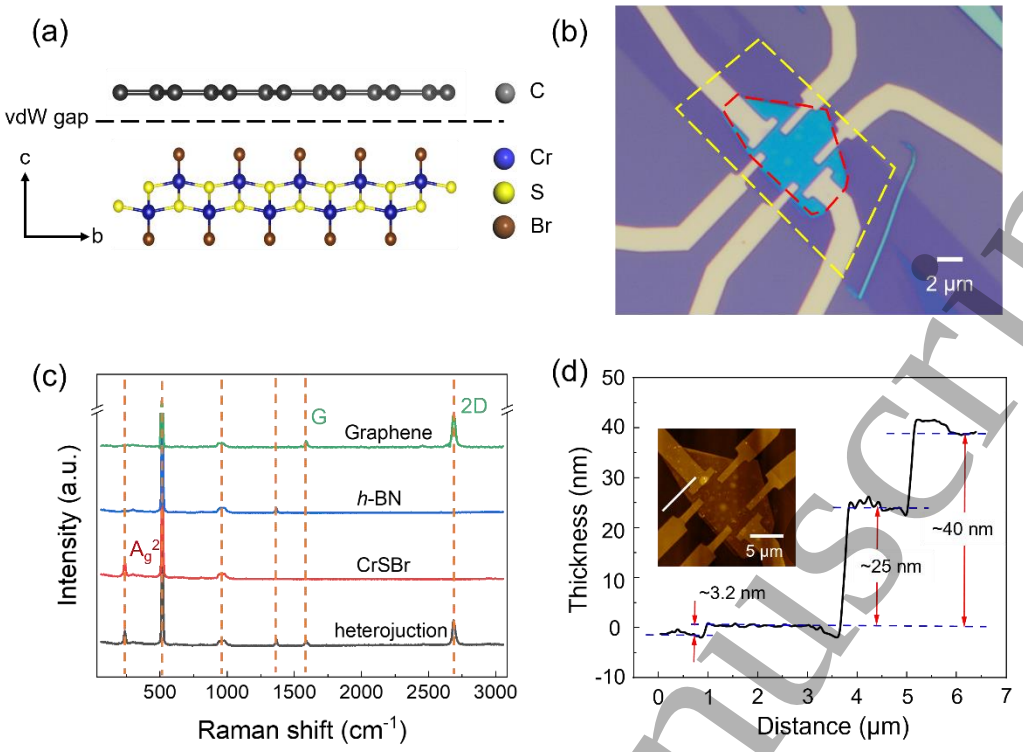

Figure 1. Structural characterizations of a graphene/CrSBr heterojunction. (a) Schematic illustration of the crystal structure of the graphene/CrSBr heterojunction. (b) Optical micrograph of the fabricated device consisting of an *h*-BN/graphene/CrSBr heterojunction on a SiO_2/Si substrate with Cr-Au electrodes. The red dash line outlines the h-BN/graphene regions, while the yellow dash line indicates the underlying CrSBr layer. (c) Raman spectra of 1L graphene, *h*-BN, CrSBr and heterojunction on a SiO_2/Si substrate. (d) The height profile along the white line of the AFM image (inset), showing a thickness of the CrSBr nanoflake (~3.2 nm), the h-BN/graphene (~25 nm), and the Cr-Au electrode (~40 nm), respectively.

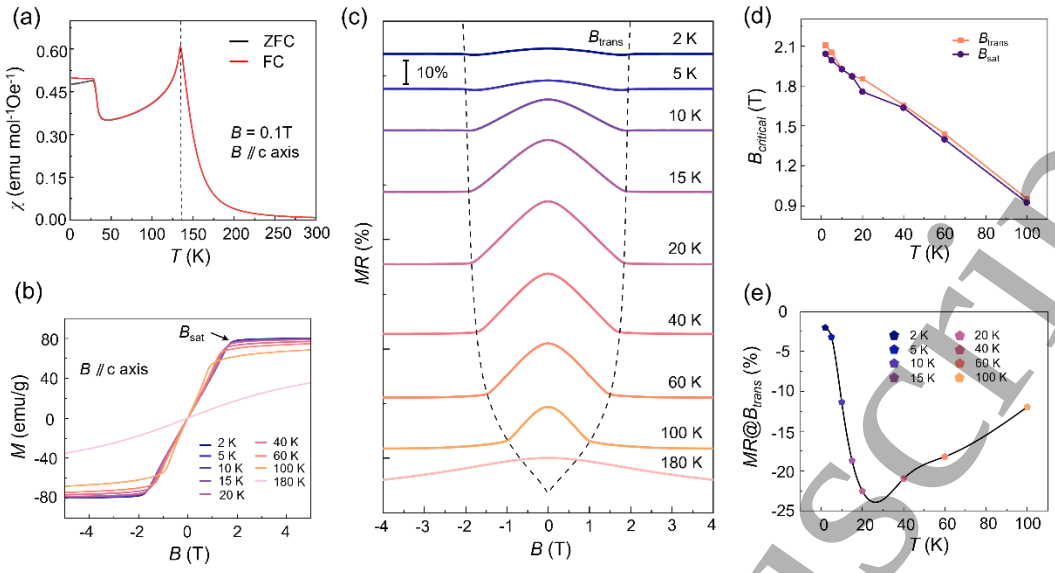

Figure 2. Magnetic properties of CrSBr and NMR of the graphene/CrSBr heterojunction. (a)Temperature-dependent magnetization of the CrSBr bulk crystal measured under an out-of-plane external magnetic field of 0.1 T. (b) Field-dependent magnetization of CrSBr at varying temperatures under out-of-plane magnetic field. (c) Magnetoresistance ratio under out-of-plane magnetic fields from −4 T to 4 T at different temperatures. The black dashed line represents the characteristic transition field, denoted as B_{trans}. (d) Comparison between the saturation field B_{sat} (purple) and the transition field B_{trans} (orange). (e) Temperature dependence of the NMR magnitude evaluated at B_{trans}.

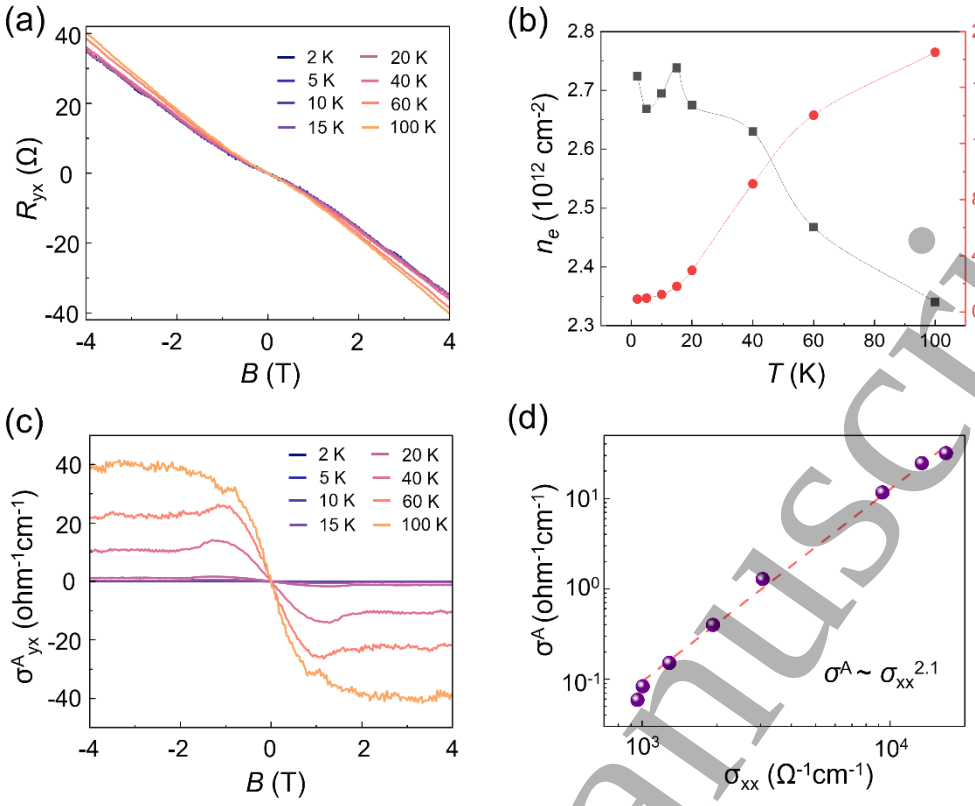

Figure 3. Anomalous Hall effect in the graphene/CrSBr heterojunction. (a) Hall resistivity R_{yx} as a function of out-of-plane magnetic field measured at various temperatures. (b) Carrier density n_e and mobility μ extracted from the high-field linear Hall response using a single-band model. (c) Temperature dependence of the anomalous Hall conductivity σ_{xy}^A. (d) Double-logarithmic plot of σ_{xy}^A versus longitudinal conductivity σ_{xx}.

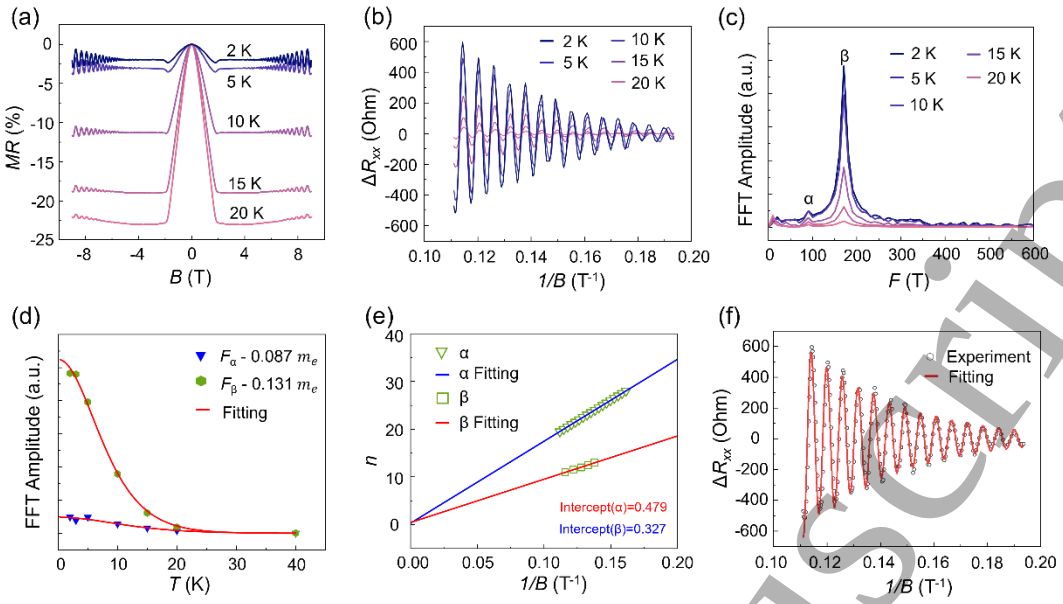

Figure 4. SdH oscillations of the graphene/CrSBr heterojunction. (a) Magnetoresistance under out-of-plane magnetic fields from −9 T to 9 T at different temperatures. (b) The oscillatory component ΔR_{xx} as the function of 1/B at various temperatures. (c) Corresponding FFT amplitude, showing the α and β frequencies. (d) Temperature dependence of the FFT amplitude of F_α (blue triangles) and F_β (green dots), fitted using LK formula to extract the effective masses. (e) Landau fan diagram and the corresponding intercepts. (f) Comparison between the experimentally extracted oscillatory component of the magnetoresistance (circles) and the theoretical simulation based on the Lifshitz-Kosevich (LK) formula (solid line).

Table 1. The derived parameters from SdH oscillations for the graphene/CrSBr heterojunction

	F(T)	K_F (Å^{-1})	A_F(nm^{-2})	m^*(m_e)	T_D (K)	τ_q (s)	μ_q (cm^{2}V^{-1}s^{-1})
α	90	0.522	0.00857	0.087m_e	42.33	2.872×10^{-14}	5.81×10^{2}
β	171	0.718	0.0163	0.131m_e	14.5	8.384×10^{-14}	1.13×10^{3}

Reference

[1] Drögeler M, Franzen C, Volmer F, Pohlmann T, Banszerus L, Wolter M, Watanabe K, Taniguchi T, Stampfer C and Beschoten B 2016 *Nano Lett.* **16** 3533–9.

[2] Banszerus L, Schmitz M, Engels S, Dauber J, Oellers M, Haupt F, Watanabe K, Taniguchi T, Beschoten B and Stampfer C 2015 *Sci. Adv.* **1** e1500222.

[3] Zatko V, Galceran R, Galbiati M, Peiro J, Godel F, Kern L-M, Perconte D, Ibrahim F, Hallal A, Chshiev M, Martinez B, Frontera C, Balcells L, Kidambi P R, Robertson J, Hofmann S, Collin S, Petroff F, Martin M-B, Dlubak B and Seneor P 2023 *Nano Lett.* **23** 34–41.

[4] Tang C, Zhang Z, Lai S, Tan Q and Gao W 2020 *Adv. Mater.* **32** 1908498.

[5] Asshoff P U, Sambricio J L, Rooney A P, Slizovskiy S, Mishchenko A, Rakowski A M, Hill E W, Geim A K, Haigh S J, Fal'ko V I, Vera-Marun I J and Grigorieva I V 2017 *2D Mater.* **4** 031004

[6] Lee J and Fabian J 2016 *Phys. Rev. B* **94** 195401.

[7] Yang H X, Hallal A, Terrade D, Waintal X, Roche S and Chshiev M 2013 *Phys. Rev. Lett.* **110** 046603.

[8] Leutenantsmeyer J C, Kaverzin A A, Wojtaszek M and Van Wees B J 2016 *2D Mater.* **4** 014001.

[9] Wei P, Lee S, Lemaitre F, Pinel L, Cutaia D, Cha W, Katmis F, Zhu Y, Heiman D, Hone J, Moodera J S and Chen C-T 2016 *Nat. Mater.* **15** 711–6.

[10] Wu Y, Yin G, Pan L, Grutter A J, Pan Q, Lee A, Gilbert D A, Borchers J A, Ratcliff W, Li A, Han X and Wang K L 2020 *Nat. Electron.* **3** 604–11.

[11] Jungwirth T, Marti X, Wadley P and Wunderlich J 2016 *Nat. Nanotechnol* **11** 231–41.

[12] Zhou B, Balgley J, Lampen-Kelley P, Yan J-Q, Mandrus D G and Henriksen E A 2019 *Phys. Rev. B* **100** 165426.

[13] Marti X, Fina I and Jungwirth T 2015 *IEEE Trans. Magn.* **51** 1–4

[14] Marti X, Fina I, Frontera C, Liu J, Wadley P, He Q, Paull R J, Clarkson J D, Kudrnovský J, Turek I, Kuneš J, Yi D, Chu J-H, Nelson C T, You L, Arenholz E, Salahuddin S, Fontcuberta J, Jungwirth T and Ramesh R 2014 *Nat. Mater.* **13** 367–74

[15] Moriyama T, Matsuzaki N, Kim K-J, Suzuki I, Taniyama T and Ono T 2015 *Appl. Phys. Lett.* **107** 122403.

[16] Che B, Hu G, Zhu C, Guo H, Lv S, Liu X, Wu K, Zhao Z, Pan L, Zhu K, Qi Q, Han,Y, Lin X, Li Z-A, Shen C, Bao L, Liu Z, Zhou J, Yang H, and Gao H-J 2024 *Chin Phys. B* 33 027502.

[17] Qiao Z, Ren W, Chen H, Bellaiche L, Zhang Z, MacDonald A H and Niu Q 2014 *Phys. Rev. Lett.* **112** 116404.

[18] Ziebel M E, Feuer M L, Cox J, Zhu X, Dean C R and Roy X 2024 *Nano Lett.* **24** 4319–29

[19] Klein J and Ross F M 2024 *J. Mater. Res.* **39** 3045–56.

[20] Guo J, Shi W, Ni K, Chen X, Liu D, Liu X, Wang S, Li Q, Xiao R-C and Yang M 2025 *Chin Phys. B* 34 104203.

[21] Shcherbakov D, Stepanov P, Weber D, Wang Y, Hu J, Zhu Y, Watanabe K, Taniguchi T, Mao Z, Windl W, Goldberger J, Bockrath M and Lau C N 2018 *Nano Lett.* **18** 4214–9.

[22] Yang B, Bhujel B, Chica D G, Telford E J, Roy X, Ibrahim F, Chshiev M, Cosset-Chéneau M and Wees B J V 2024 *Nat. Commun.* **15** 4459.

[23] Scheie A, Ziebel M, Chica D G, Bae Y J, Wang X, Kolesnikov A I, Zhu X and Roy X 2022 *Adv. Sci.* **9** 2202467.

[24] Beck J 1990 *Z. Anorg. Allg. Chem.* **585** 157–67.

[25] Pizzocchero F, Gammelgaard L, Jessen B S, Caridad J M, Wang L, Hone J, Bøggild P and Booth T J 2016 *Nat. Commun.* **7** 11894.
[26] Ye C, Wang C, Wu Q, Liu S, Zhou J, Wang G, Söll A, Sofer Z, Yue M, Liu X, Tian M, Xiong Q, Ji W and Renshaw Wang X 2022 *ACS Nano* **16** 11876–83.
[27] Telford E J, Dismukes A H, Lee K, Cheng M, Wieteska A, Bartholomew A K, Chen Y, Xu X, Pasupathy A N, Zhu X, Dean C R and Roy X 2020 *Adv. Mater.* **32** 2003240.
[28] Telford E J, Dismukes A H, Dudley R L, Wiscons R A, Lee K, Chica D G, Ziebel M E, Han M-G, Yu J, Shabani S, Scheie A, Watanabe K, Taniguchi T, Xiao D, Zhu Y, Pasupathy A N, Nuckolls C, Zhu X, Dean C R and Roy X 2022 *Nat. Mater.* **21** 754–60.
[29] Wang X, Yang Y, Li Y, Liu G, Duan J, Wang Z, Lu L and Yang F 2025 *Phys. Rev. B* **112** 165204.
[30] Li C-Z, Wang L-X, Liu H, Wang J, Liao Z-M and Yu D-P 2015 *Nat. Commun.* **6** 10137.
[31] Karki Chhetri S, Acharya G, Graf D, Basnet R, Rahman S, Sharma M M, Upreti D, Nabi M R U, Kryvyi S, Sakon J, Mortazavi M, Da B, Churchill H and Hu J 2025 *Phys. Rev. B* **111** 014431.
[32] Liu H, Xue Y, Shi J-A, Guzman R A, Zhang P, Zhou Z, He Y, Bian C, Wu L, Ma R, Chen J, Yan J, Yang H, Shen C-M, Zhou W, Bao L and Gao H-J 2019 *Nano Lett.* **19** 8572–80.
[33] Qi Q, Lv S, Zhu K, Xie Y, Hu G, Zhao Z, Xian G, Han Y, Yang Y, Bao L, Lin X, Guo H, Yang H, and Gao H-J 2025 *Chin Phys. B* 34 077305.
[34] Fu Y, Zhao N, Chen Z, Yin Q, Tu Z, Gong C, Xi C, Zhu X, Sun Y, Liu K and Lei H 2021 *Phys. Rev. Lett.* **127** 207002.
[35] Ding L, Koo J, Yi C, Xu L, Zuo H, Yang M, Shi Y, Yan B, Behnia K and Zhu Z 2021 *J. Phys. D: Appl. Phys.* **54** 454003.
[36] Liang T, Gibson Q, Ali M N, Liu M, Cava R J and Ong N P 2015 *Nat. Mater.* **14** 280–4.
[37] Mikitik G P and Sharlai Yu V 1999 *Phys. Rev. Lett.* **82** 2147–50.
[38] Luk'yanchuk I A and Kopelevich Y 2004 *Phys. Rev. Lett.* **93** 166402.
[39] Xiang F-X, Wang X-L, Veldhorst M, Dou S-X and Fuhrer M S 2015 *Phys. Rev. B* **92** 035123.
[40] Rassekh M and Gmitra M, 2026 *Phys. Rev. B* 113 035126.
[41] Mao R, Feng Z and Li Z, 2026 *Appl. Surf. Sci.* 732 166508.